Origin of magnetic circular dichroism in soft x-ray fluorescence of Heusler alloys at threshold excitation

M. V. Yablonskikh,[1,*] Yu. M. Yarmoshenko,[2] V. I. Grebennikov,[2] E. Z. Kurmaev,[2] S. M. Butorin,[1] L.-C. Duda,[1] J. Nordgren,[1] S. Plogmann,[3] and M. Neumann[3]

[1]*Physics Department, Uppsala University, Box 530, S-75121 Uppsala, Sweden*

[2]*Institute of Metal Physics, Russian Academy of Sciences—Ural Division, 620219 Ekaterinburg GSP-170, Russia*

[3]*Universität Osnabrück, Fachbereich Physik, D-49069 Osnabrück, Germany*

(Received 22 February 2000; revised manuscript received 4 October 2000; published 1 June 2001)

The results of investigations of the Heusler alloys NiMnSb and Co_2MnSb by magnetic circular dichroism in soft x-ray emission spectroscopy (SXEMCD) are presented. The data obtained are in a good agreement with theoretical calculations of x-ray emission. A very intense resonant inelastic peak in the Mn L_3 spectra in the region of states above the nominal Fermi level was observed and attributed to x-ray reemission. The interplay between the theoretically predicted half-metallic character of the Mn $3d$ valence band and the Mn L_2,L_3 SXEMCD spectra is discussed.

DOI: 10.1103/PhysRevB.63.235117 PACS number(s): 78.70.En, 75.25.+z, 75.20.Hr, 87.64.Ni

I. INTRODUCTION

X-ray magnetic circular dichroism (MCD) was predicted by Erskine and Stern.[1] Circularly polarized core-level photoabsorption and photoemission in magnetic systems have recently attracted much attention, both experimentally and theoretically, following the observation of linear magnetic dichroism in rare-earth materials by van der Laan *et al.*[2] The existence of magnetic circular dichroism in absorption of circularly and linearly polarized radiation was experimentally demonstrated by Schnütz *et al.* in a large number of rare-earth and transition metal systems.[3,4] Magnetic dichroism in x-ray absorption (XA) is considered to be a standard technique that was initially applied to study the fine structure of empty electronic states in a conduction band and their spin configuration. The absorption of polarized x rays creates core holes with different orbital and spin projections, depending on the polarization and excitation energy of the incoming photons. That is directly connected through sum rules to the spin-angular-momentum-dependent hole population of the valence shell in the ground state.[5,6]

Soft x-ray emission (SXE) spectroscopy is known to be an element-selective probe of electronic structure, related to the occupied partial density of states. It has been shown that the spin-polarized core hole created by the incident photon may be used as a local site-specific spin detector for the valence states via appropriate valence-to-core hole transitions.[7] According to these expectations, the MCD effect can be observed without detecting the polarization of emitted photons if core holes are excited alternately by right- and left-handed circularly polarized radiation relative to the sample magnetization direction. In this case the difference in the emitted radiation (later referred to as the magnetic dichroism spectrum) closely reflects the spin-resolved local density of states (DOS).

Regarding the question of how the electronic structure of localized magnetic systems influences the x-ray emission spectra, we emphasize two factors that make things complicated. The first is the rather small number of experiments using the SXEMCD technique, especially for localized magnets.[8] X-ray emission spectroscopy (XES) as an experimental technique has not been as greatly developed as x-ray absorption, because it is more complicated with respect to experimental apparatus as well as in the theoretical description.[7] The SXEMCD technique became a subject of study recently after Strange *et al.* predicted the dependence of Fe L_3 XES on the relative alignment of the polarization vector of the incoming excitation beam and the sample magnetization.[9] SXEMCD measurements have been done for Fe L_2,L_3 using nonmonochromatized synchrotron radiation[10] and monochromatic excitation.[11] Fe, Co, and Ni films,[12] $Rh_{25}Fe_{75}$,[13] and Fe-Co alloys[14] have also been investigated.

The second complicating factor is that theories describing the phenomenon of MCD in x-ray emission are apparently being reconsidered. We found several theoretical approaches to describing magnetic dichroism in x-ray emission spectroscopy,[15–18] but they seem to be insufficient to describe the experimental data. Pustogowa *et al.*[15] described x-ray emission as a first-order process in perturbation theory, considering x-ray emission independently from the absorption of excited photons. These authors considered the difference in intensities of emitted photons with right- and left-handed polarization, which is opposite to the polarization of the measured x-ray spectra in our case. In Ref. 16 the dichroism of x-ray fluorescence spectra was investigated at high energy excitation far above threshold. In a recent paper[17] giving a basic treatment of x-ray emission the interconversion of spin direction for the spin orbit split $2p_{1/2}$ and $2p_{3/2}$ shells was neglected. This model was improved by Kuiper.[18] However, he worked with atomic functions and obtained only integrated intensities of XES. In our approach, we consider the difference between polarization integrated emission spectra excited with left- and right-polarized incoming photons, which is close to the experimental. As well as the normal x-ray emission generating the final valence hole,[20] an appropriate model has to consider other decay channels of the core hole created. To take into account

$3d4s \rightarrow 2p$ x-ray transitions from occupied and unoccupied Mn $3d$ states also, we were forced to develop a theory and put it forward for discussion by the scientific community.

In order to investigate magnetic circular dichroism applied to localized magnetic systems a pair of ''classic'' Mn-based Heusler alloys[21] was selected. Co_2MnSb has an $L2_1$ lattice and NiMnSb has a $C1_b$ lattice.[22] These Heusler alloys (HA's) have magnetic moments of about (3.3–4) μ_B localized on the Mn atoms, and they are traditionally considered as having strongly localized $3d$ electrons, so experimental studies of the energy distribution of the Mn $3d$ states are of great importance. Band calculations[23] for HA's show that the majority-spin Mn $3d$ states are occupied. For the minority-spin states, the Mn $3d$ band is empty and positioned at 1–1.5 eV above the Fermi level in most cases. Studies of the electronic structure of HA's intensified after the theoretical prediction of a half-metallic ferromagnetic (HMF) state,[23] i.e., a nonzero density of states at the Fermi level in one spin channel and a band gap in the other in NiMnSb and PtMnSb alloys. Band calculations[19,24] show that a state close to HMF may exists also in Co_2MnZ (Z=Al,Si,Ga,Sn) alloys.

A correlation between the energy splitting of the Mn $2p_{3/2}$ core level and the value of the local magnetic moment was observed by x-ray photoemission spectroscopy.[25] This is due to the strong $2p$-$3d$ exchange interaction within the Mn $3d$ band, which also affects the shape of Mn $L_{2,3}$ XE spectra and their relative intensity ratio $I(L_2)/I(L_3)$.[26] Here we use SXEMCD to study the spin-resolved Mn $3d$ partial density of states by measuring the same $3d4s \rightarrow 2p$ x-ray emission spectra.

The outline of this paper is as follows. First, we describe experimental details (Sec. II A) and characteristic features of the observed spectra (Sec. II B). Then we give a brief description of our theoretical approach and spectra formation mechanism (Sec. II C). The comparison between experiment and theory (Sec. II D) results in some conclusions (Sec. III). Details of the mathematical formalism are outlined in the Appendix.

II. RESULTS AND DISCUSSION

A. Experimental details

The experiment was performed at the helical undulator beamline ID12B at the European Synchrotron Radiation Facility (ESRF) in Grenoble, France[27,28] which is a high-brightness third-generation high-energy synchrotron source. This beamline consists of a Dragon-like spherical grating monochromator producing some 83% circularly polarized x rays. The extraordinarily low emittance of the 6 GeV stored electron beam allowed us to refocus the x-ray beam that passes the monochromator exit slit into a spot with dimensions of about $40\,\mu\text{m} \times 1$ mm without excessive loss of intensity. It is of crucial importance to achieve the smallest attainable focal spot in order to collect as much of the fluorescence signal with the x-ray emission spectrometer[29] as possible. The energy spread of the excitation beam was set to about 0.9 eV full width at half maximum (FWHM) in order to have reasonable acquisition times (several hours, depending on excitation energy).

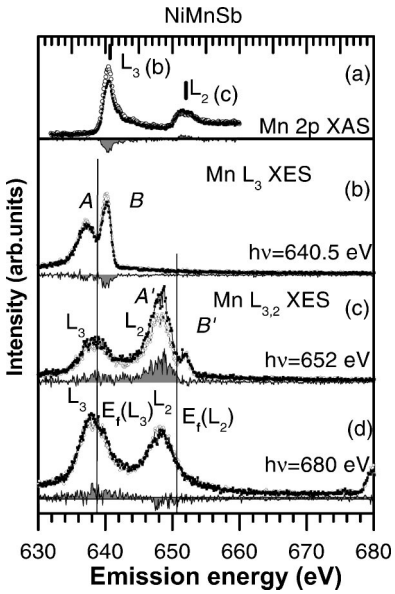

FIG. 1. The Mn L_2,L_3 XES following energy-dependent excitation for monocrystalline NiMnSb. Shown are Mn $2p$ XAS (a) and XES (b,c,d) spectra excited with parallel alignment of the incoming photon helicity and sample spin moment (filled squares) and antiparallel alignment (open circles). Difference spectra are indicated by the black solid line. The Mn $2p_{3/2}$ and Mn $2p_{1/2}$ binding energies relative to the Fermi level are labeled $E_f(L_3)$ and $E_f(L_2)$, respectively.

The samples were magnetized by using two Nd-Fe-B magnets situated in vacuum, directly behind the samples (essentially a horseshoe configuration with a few millimeters air gap). The field strength was about 0.2 T (estimated) at the sample site. The magnets were attached to the axis of a vacuum-compatible rotational stepper motor to facilitate a reversal of sample magnetization. The samples remained in a fixed position during the entire data acquisition. After every 10 min, data acquisition in a certain geometry, say, coparallel alignment of photon helicity and magnetization, was suspended and the magnetization was reversed to antiparallel alignment by activating the motor. This procedure took about 2 s, after which data acquisition in the reverse geometry was resumed, and the entire cycle was repeated for several hours. The time lag between the two geometries was negligible due to the very long lifetime (more than 35 h) of the stored electron beam. The magnetic field was parallel to the incident x rays, which were incident on the sample at 5° to the surface. The optical axis of the spectrometer was adjusted to coincide with the surface normal. The spectral resolution was 0.7 eV. A single crystal of NiMnSb and a polycrystalline sample of Co_2MnSb were used for x-ray fluorescence measurements in vacuum ($10^{-8} \times 10^{-9}$ Torr). The samples were scraped in a vacuum of 10^{-6} Torr before the measurements.

B. Characteristic features of spectra

For brevity, we shall mainly discuss the XE spectra of NiMnSb. Figure 1(a) contains Mn $L_{2,3}$ absorption and Mn $L_{2,3}$ fluorescence spectra of NiMnSb. The spectra have been induced by circular right-hand (photon helicity is parallel to

the spin momentum of the sample) and left-hand (antiparallel) polarizations. For XAS [Fig. 1(a]) we observed dichroism that reaches a maximum at the L_3 absorption edge (negative sign of the difference) and a smaller one at the L_2 absorption edge (positive sign). According to Ref. 30 the absolute value of the dichroic difference can be increased by applying a larger external magnetic field. The curves (b), (c), and (d) in Fig. 1 show Mn $L_{2,3}$ x-ray emission spectra obtained at different excitation energies. The following features can be seen in the Mn L_3 spectrum excited at $E_{exc}=640.5$ eV [Fig. 1(b)]. There are three effects in the spectrum: (i) the spectrum consists of two bands with maxima at 637.5 eV (peak A) and at 640.5 eV (peak B), (ii) both bands have dichroism of the same sign, coinciding with that at the L_3 absorption edge, and the maximal dichroism in x-ray emission is at 640.5 eV photon energy, which also coincides with the energy position of the L_3 absorption edge, and (iii) an anomalously high peak B (in comparison to the normal emission peak A) is observed. We suggest that the high intensity of peak B is explained by the sum of the elastic scattering contribution and the substantial radiative transition of electrons with energies higher than the Fermi energy, i.e., by the relaxation of the intermediate state with electron configuration $2p^5 3d^{n+1}$, which involves contributions from the $3d$ states nominally vacant in the ground state configuration.

The Mn x-ray emission spectrum at the L_2 threshold energy of 652 eV is presented in Fig. 1(c). First, we note that the L_3 peak B ($E=640.5$ eV) does not disappear completely due to reemission but merges with the normal emission peak A (details will be explained in the next section). Both peaks form the L_3 spectrum. Second, no dichroism is observed at the B' resonance peak. The absolute intensity of the B' peak is much lower than that of peak A', which is opposite to the intensity ratio $I(A)/I(B)$ at $E_{exc}=640.5$ eV. Note that in a larger external magnetic field the dichroism at the L_3 and L_2 lines may be increased. The dichroism of the A' peak is very large in comparison with that at both the emission peak B [Fig. 1(b)] and the absorption peak L_2 [Fig. 1(a)—see also the MCD spectral values aligned to the Fermi level in Fig. 3 below].

Mn L_3 and L_2 x-ray emission lines excited at energies far above the threshold $E_{exc}=680$ eV are shown in Fig. 1(d). The dichroism at L_3 and L_2 has different signs, opposite to the cases of near-threshold excitations [Figs. 1(b) and 1(c)]. L_3 x-ray emission from states nominally above the Fermi level and a high $I(L_2)/I(L_3)$ intensity ratio for Mn L_2,L_3 spectra relative to pure Mn are observed. This is in good agreement with XES obtained by electron excitation.[26] Similar spectral features were observed for Cr L_3,L_2 XES of Cr-intercalated systems, where the high magnetic moment at the Cr site is related to the strong localization of Cr $3d$ states and the predicted band gap.[31]

The Mn $L_{3,2}$ XES of polycrystalline Co_2MnSb are presented in Fig. 2. The same behavior of Mn emission for corresponding excitation energies is apparent for NiMnSb and Co_2MnSb.

Let us discuss in more detail the spectra in Fig. 2(b) corresponding to an intermediate excitation energy value of

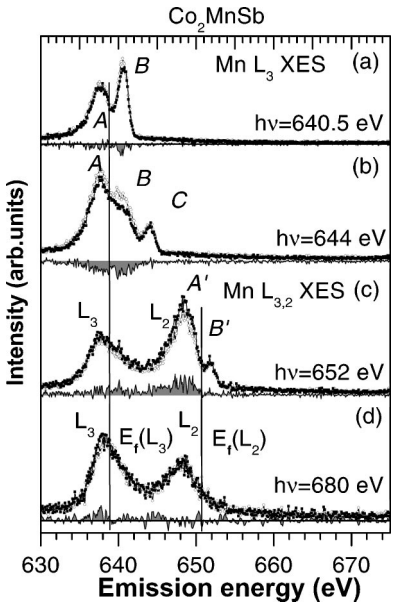

FIG. 2. The Mn L_2,L_3 XES following energy-dependent excitation for polycrystalline Co_2MnSb. All designations are the same as for Fig. 1. The Mn $2p_{3/2}$ and Mn $2p_{1/2}$ binding energies relative to the Fermi level are indicated as $E_f(L_3)$ and $E_f(L_2)$, respectively.

$E_{exc}=644$ eV. The elastic scattering peak C exhibiting no dichroism is situated apart from the Mn L_3 x-ray emission lines A and B. From comparison of Fig. 2(a) and Fig. 2(b) one can see the coincidence between the dichroism maxima at 640.5 eV. Apparently, the peak B in spectrum (b) arises due to the relaxation of an excited electron into a long-life time state (a trap) above the Fermi energy and then a fluorescence transition to the $2p_{3/2}$ level.

Smoothed dichroism spectra of NiMnSb and of Co_2MnSb are presented in Figs. 3 and 4. The spectra are shifted to the Fermi energy, using the corresponding $2p$ core-level energies obtained from XPS measurements.[26] For both alloys dichroism of the same sign is observed for Mn L_3 XES measured at L_3 threshold excitation [Figs. 3(b) and 4(a)] and for Mn L_2 XES measured at L_2 threshold excitation [Figs. 3(c) and 4(c)]. Moreover, the sign of the Mn L_3 XE dichroism intensity is negative in the case of L_3-edge resonant excitation, while that for Mn L_2 is positive in the case of L_2-edge resonant excitation. Thus, the XE dichroism intensities follow the XA dichroism intensities at corresponding excitation energies (Fig. 1). The high level of noise in cases of excitation far above the L_2,L_3 thresholds with photon energy $E_{exc}=680$ eV makes it difficult to confirm the difference between XE dichroism spectra [Figs. 1(d) and 2(d)].

C. The model of resonant x-ray scattering

The main features of the electronic structure of Heusler alloys can be seen using the $3d$ Mn spin-resolved density of states. The current calculation (see Fig. 5) is taken from Ref. 32. Spin-down states are prevalent above the Fermi energy. They form a narrow peak at 1–1.5 eV above the Fermi energy. In the filled part of the Mn $3d$ DOS, the spin-up states dominate. These features also influence the x-ray transitions.

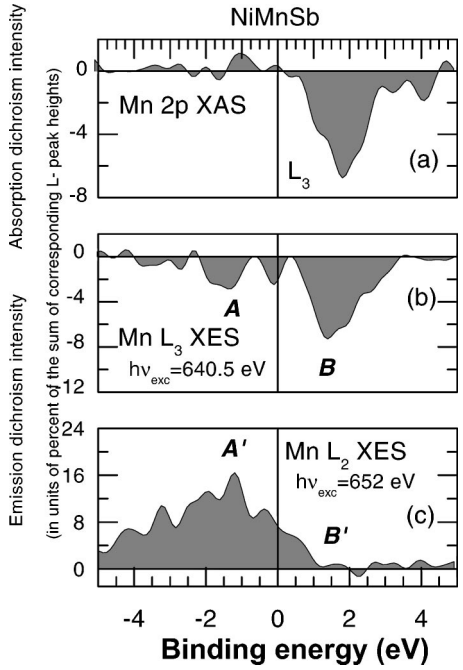

FIG. 3. Emission dichroism intensity for NiMnSb. Difference spectra are shifted to Fermi level according to experimental core-level energies (Ref. 26). Labels A,A',B,B' correspond to labels in Fig. 1.

We developed a theoretical model describing resonant (with the core-level excitation) scattering of polarized x rays in terms of the Mn $3d$ DOS, which is specific for the Mn-based Heusler alloys investigated. The mathematical formalism is

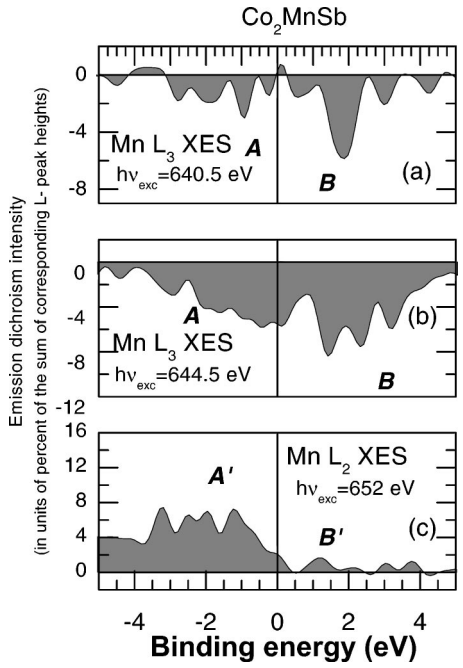

FIG. 4. Emission dichroism intensity for Co_2MnSb. Difference spectra are shifted to Fermi level according to experimental core-level energies (Ref. 26). Labels A,A',B,B' correspond to labels in Fig. 2.

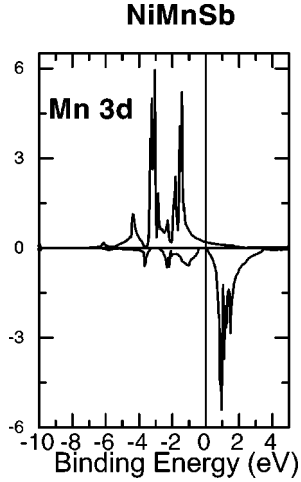

FIG. 5. Mn $3d$ spin-polarized density of states for NiMnSb (Ref. 32).

given in the Appendix. Here only the main aspects of the theory are discussed.

The simplest approach is to consider x-ray absorption and emission as two independent processes, but often this will not work, because the emission process starts from excited valence states and not from the ground state. Let us consider an excited core-level electron, which is added to the valence electrons as the result of incoming photon absorption. The excited electron can (i) leave the excited atom, (ii) lose its energy and mingle in the crowd of other valence electrons, or (iii) return to the empty core level with radiation of an x-ray quantum. The process (iii) is known as reemission. Usually, the reemission contribution to the spectra of metals is not large, compared to concurrent processes. Therefore, the reemission peak usually looks like a small tail on the Fermi energy side. It is a fundamental claim of our work that the reemission in metallic Heusler alloys is anomalously large in Mn L_3 XES for several reasons.

The model is based on the partial $3d$ density of states of NiMnSb (Fig. 5) which has the following main features: (i) a strong (about 2 eV) exchange interaction rather than a weak spin-orbit interaction forms the band states; (ii) spin-down states have a strong peak above the Fermi level (spin-up states are absent in this region; they are located below the Fermi level). That spin-down peak acts as a spin-selective trap for excited core-level electrons. The presence of the energy gap between filled and empty states is also important. It makes it possible to observe and clearly distinguish x-ray reemission and x-ray emission contributions to the Mn $L_{2,3}$ XES.

Let us discuss the origin of dichroism. Core states are split by the spin-orbital interaction into $2p_{3/2}$ and $2p_{1/2}$. In the $2p_{3/2}$ states, the orbital and spin moments are roughly parallel, while in $2p_{1/2}$ they are antiparallel. The spin direction is fixed by spin polarization of the empty states, where a

core-level electron is excited under absorption of an x-ray quantum. In this way the states with orbital moment projections parallel (or antiparallel) to the spin moment of the atom are selected. The photons with right (photon helicity $+1$, parallel to the atomic spin moment) and left (photon helicity -1, antiparallel) polarizations interact differently with electrons having a fixed projection of the orbital moment. This leads to dichroism. X-ray emission is the reverse process with respect to x-ray absorption and therefore also shows dichroism. Using the second order theory of electron-photon interaction we give a quantitative description of emission, reemission, and absorption within the one-particle approach (see the Appendix).

To simplify the equations, the orbital angular momentum energy distribution in the d band is neglected. We take into account the exchange energy splitting of spin states only. In addition, we consider that the polarization of emitted x rays has equal projections on all three axes in a coordinate system connected with the sample magnetization. This is true at the ''magic'' angle 55° between the photon direction and the magnetization axis, and it is reasonable for our experimental geometry. The $L_{2,3}$ emission intensities following x-ray excitation with energy $h\nu$ and polarization $q=\pm 1$ are given by the equations

$$^{1/2}I_q^e(\epsilon')\propto\frac{1}{\Gamma_x}\{6g_s(\epsilon')g_s(\epsilon)+0.8g_a(\epsilon')g_a(\epsilon)+q[-g_a(\epsilon')g_s(\epsilon)-3g_s(\epsilon')g_a(\epsilon)]\},\quad(1)$$

$$^{3/2}I_q^e(\epsilon')\propto\frac{1}{\Gamma_x}\{12g_s(\epsilon')g_s(\epsilon)+6.8g_a(\epsilon')g_a(\epsilon)+q[5g_a(\epsilon')g_s(\epsilon)+3g_s(\epsilon')g_a(\epsilon)]\}.\quad(2)$$

Here $\epsilon=h\nu-|E_{2p_j}|-i\Gamma_x$ and $\epsilon'=h\nu'-|E_{2p_j}|-i\Gamma_f$ are the energies of excited band electrons after photon absorption and after emission of the quantum $h\nu'$, respectively; $g_{s,a}(\epsilon)=[g^{\uparrow}(\epsilon)\pm g^{\downarrow}(\epsilon)]/2$ are the charge and spin components of the partial DOS calculated per one d state per atom. They are smoothed by the widths of intermediate Γ_x and final Γ_f states.

In the same units, the reemission (elastic scattering) contribution is given by

$$^{1/2}I_q^r(\epsilon)\propto\frac{1}{\Gamma^*}[4g_s^2(\epsilon)+g_a^2(\epsilon)-q\times 4g_s(\epsilon)g_a(\epsilon)],\quad(3)$$

$$^{3/2}I_q^r(\epsilon)\propto\frac{1}{\Gamma^*}[16g_s^2(\epsilon)+g_a^2(\epsilon)+q\times 8g_s(\epsilon)g_a(\epsilon)],\quad(4)$$

where Γ^* is the inverse lifetime of intermediate resonance states. Equations (1)–(4) describe the emission spectra following x-ray excitation with energy $h\nu$ and polarization $q=\pm 1$ with respect to the sample magnetization in terms of the charge and spin density of empty and filled d states. After integration over the d band we get the result of Ref. 18. The form of the absorption spectra is

$$^{1/2}I_q^a(\epsilon)\propto[2g_s(\epsilon)-qg_a(\epsilon)],\quad(5)$$

$$^{3/2}I_q^a(\epsilon)\propto[4g_s(\epsilon)+qg_a(\epsilon)].\quad(6)$$

The x-ray hole appearing at the core level creates a potential that acts on other electrons in the excited atom. The effective value of the potential $U\approx 2$ eV can be simply evaluated by division of the unscreened Coloumb interaction energy of two elementary charges (about 10 eV) by the number of Mn $3d$ electrons. This core-hole field turns on suddenly and shakes up the valence electrons.[33–35] But first we consider the ground state of the electrons (full relaxation case) in this core-hole field. This state is described by the so-called impurity DOS, which can contain a local electron level, separate from the d band. Let us turn to the spin-down band in the Mn $3d$ DOS, Fig. 5. The peak above the Fermi energy gives the main contribution to the reemission process. These states are shifted down in the core-hole field by about the value of U. As a result, the peak may shift down below the Fermi level, thus leading to an increase of the electron lifetime in the excited state.

Another core-hole effect is also significant. Besides the ground state, contributions from the excited states can be essential. In magnetic materials, first of all, one should take into account states with a reversed local magnetic moment at an excited atom. The spin-reversal energy is of the order of 0.1 eV, i.e., the Curie temperature. This is small as compared to $U=2$ eV. Such spin-flip excitations suppress the observed values of dichroism and should be taken into account in the analysis of experimental data.

D. Discussion

For the quantitative theoretical analysis of experimental spectra we use the formulas (1)–(6). We take $I^e(\epsilon')=[I_+^e(\epsilon')+I_-^e(\epsilon')]/2$ at a fixed energy of excitation, i.e., the spectrum averaged over the polarization of the incoming radiation, for the description of the emission spectrum. The difference spectrum (dichroism of emission) can be described as $DI^e(\epsilon')=[I_+^e(\epsilon')-I_-^e(\epsilon')]/2$. Let us introduce similar formulas for the reemission and absorption spectra.

Under threshold excitation energy, core-level electrons are transferred to the empty peak of the DOS (at ~ 1–1.5 eV; see Fig. 5), the spin polarization of which, $P^e=g_a(\epsilon)/g_s(\epsilon)$, is taken equal to -1. The polarization of filled states located below the Fermi level is $P^f=0.5$. In case of excitation with high energy far away from the threshold we assume $P^e=0$. Finally, we take into account a higher damping of the excited resonance state in reemission by setting $\Gamma^*=2\Gamma_x$.

The results of the intensity calculation for normal x-ray emission I^e [in units of $(1/\Gamma_x)g_s(\epsilon')g_s(\epsilon)$], reemission I^r [in units of $(1/\Gamma_x)g_s^2(\epsilon)$] and absorption [in units of $g_s(\epsilon)$] are given in Table I together with corresponding MCD intensities. Looking at the DOS in Fig. 5, one can see that $g_s(\epsilon')\approx g_s(\epsilon)$ for the main peaks below and above the Fermi energy ϵ_f. So the threshold emission and reemission intensities are given in the same units. The first two lines correspond to the threshold excitation of an electron from the

TABLE I. Intensities of x-ray emission I^e [in units of $(1/\Gamma_x)g_s(\epsilon')g_s(\epsilon)$], reemission I^r [in units of $(1/\Gamma_x)g_s^2(\epsilon)$], and absorption I^a [in units of $g_s(\epsilon)$] and corresponding MCD intensities DI for L_2,L_3 spectra. P^f and P^e are spin polarization of filled and empty states

Φ_c	P^f	P^e	I^e	DI^e	I^r	DI^r	I^a	DI^a
$2p_{1/2}$	0.5	-1	5.6	2.5	2.5	2	2	1
$2p_{3/2}$	0.5	-1	8.6	-0.5	8.5	-4	4	-1
$2p_{1/2}$	0.5	0	6	-0.5	2	0	2	0
$2p_{3/2}$	0.5	0	12	2.5	8	0	4	0

L_2 ($2p_{1/2}$) and L_3 ($2p_{3/2}$) levels, $P^e=-1$, and the last two lines correspond to excitation far away from the thresholds, $P^e=0$. In the latter case, the quantities I^r and DI^r have a rather nominal character, because the actual relaxation Γ^* in high energy states is much stronger than that taken into account in calculations and, moreover, $g_s(\epsilon') \ll g_s(\epsilon)$.

Comparison of the calculations given in Table I with experimental spectra (Figs. 1 and 2) shows reasonable agreement. According to the calculation, absorption at the L_3 edge is related to that at the L_2 edge as 4:2; moreover, the dichroism of the L_3 absorption is negative (-1) while that of the L_2 edge is positive $(+1)$ which is qualitatively (in sign) in agreement with the observed spectrum (see Fig. 1) (note that the orbital angular momentum distribution is neglected in our simple approach). The calculated reemission/emission intensity ratios at the L_3 and L_2 thresholds are 8.5/8.6 and 2.5/5.6, respectively, and the signs of the dichroism are found to be the same for reemission and emission at the L_3 threshold (with different values: -4 for reemission, and -0.5 for emission). The same behavior is seen for experimental spectra. In contrast, the dichroism of normal XES at the L_2 threshold (2.5) is higher than that of reemission at L_2 (2.0).

Finally, the theory explains the change in sign of the dichroism for both emission L_2 and L_3 lines when going from near-threshold excitation ($P^e=-1$) to excitation far above the threshold ($P^e=0$). Such a change of the dichroism sign can be explained within a two-step process of x-ray emission. First, a core-level electron goes to an empty state. This process is characterized by dichroism of absorption. Then, normal emission takes place (with an x-ray transition from the valence band to the core-level hole) which is characterized by dichroism of emission (due to polarization of the filled valence states). In the case of near-threshold excitation, both these constituents of dichroism have different signs because the spin polarizations of the empty and filled states are different. In this case, the dichroism of the first process (absorption) prevails. For excitation far away from the threshold, the empty states are nonpolarized, and the result is determined by the dichroism of the second step, i.e., emission.

Let us consider these quantitative results more carefully. Note that the calculated dichroism is higher than the observed one. This is for two reasons, experimental and theoretical. Measurements of the difference spectra were performed under not completely optimal conditions: the external magnetic field was rather small and the statistics of low-intensity lines was sometimes insufficient for quantitative estimations. On the other hand, as noted above, the one-particle approach does not take into account the peculiarities of the electron system connected with the possibility of transitions to the excited states. The process of atomic spin reversal is the most destructive for dichroism. This point must be taken into account in a quantitative comparison of one-particle calculations with experimental data.

Going back to the reemission elastic peaks at the L_3 and L_2 thresholds [Figs. 1(b) and 1(c)], we need to note that the relative intensity of the first one is much higher than that of the second. Although the calculations predict a decrease of the I^r/I^e ratio from 1.0 to 0.45 when going from the L_3 to the L_2 threshold, the observed reemission peak at the L_2 threshold is much smaller. This might be due to the shorter lifetime of the L_2 core hole (with respect to that of the L_3 core hole) as a result of an additional Coster-Kronig transition. One can also suppose that the field of the L_2 core hole with higher binding energy is more strongly screened than that of the L_3 core hole. The value of the field directly defines the lifetime of the excited electron at the central atom and hence the reemission probability. The spectra measured at the L_3 threshold are more intense than those at the L_2 threshold because the L_3 level is also excited by the Coster-Kronig transition under excitation of the L_2 level, and a superposition of two spectra takes place.

Formulas (1) and (2) allow us to understand the increase of the the L_2/L_3 ratio with the increase of spin polarization, or, the same thing, with the increase of the atomic magnetic moment. In this process, the absolute value of the negative product $g_a(\epsilon')g_a(\epsilon)$ grows (the spin polarizations of empty and filled states are opposite), which leads to the weakening of both emission lines with increasing spin polarization. However, the suppression of the L_3 emission is much higher [the coefficient in Eq. (2) is 6.8] than the suppression of the L_2 emission [the coefficient in Eq. (1) is 0.8]. In the extreme case of 100% polarization of empty and filled states one obtains $^{1/2}I^e = {}^{3/2}I^e$.

The reason is a restriction of some transitions due to the spin selection rules. Only two states of the $2p_{3/2}$ shell (out of four) take part in transitions, i.e., the same as in the $2p_{1/2}$ shell. The selection rule is illustrated by Fig. 6 for $2p_{3/2}$ states with maximal degree of polarization. The extreme situation was observed for the half-metallic DOS. The $|3/2,3/2\rangle$ state has majority-spin (spin-up) polarization and excitation of this inner state is forbidden, because there is no spin-up density of states above the Fermi level. The electron in the $|3/2,-3/2\rangle$ minority-spin state can be excited above the Fermi level, but the emission transition of an electron below E_F is again forbidden because there are no spin-down states below E_F, so the process stops at the emission step.

III. SUMMARY

It was shown in experiment and by theoretical considerations that the magnetic structure of a system strongly affects both circular dichroism and the intensity distribution of x-ray emission spectra obtained at different excitation energies. The investigation of x-ray emission valence spectra of Mn

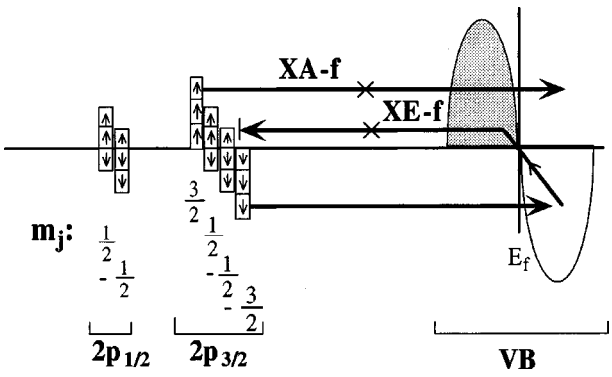

FIG. 6. The fluorescence transition scheme $2p \rightarrow 3d$ for ultimate polarization of the valence band. An excitation of the state $|3/2,3/2\rangle$ with majority-spin electron is forbidden (XA-f). The electron in the minority-spin state $|3/2,-3/2\rangle$ can be excited above the Fermi level, but the normal emission transition of the electron with energy below E_F is forbidden (XE-f).

demonstrates an anomalously high ratio $I(L_2)/I(L_3)$ of emission line intensities as compared to that in pure $3d$ metals. This is related to the high degree of spin polarization of valence states in half-metallic ferromagnets. A large magnetic dichroism effect was found in the Mn L_2,L_3 x-ray emission spectra. That indicates a strong exchange splitting between spin-up and spin-down Mn $3d$ states.

An x-ray reemission peak originating from the states above the Fermi energy was found in Mn L_3 XES in Mn-based Heusler alloys. The energy position of this peak exactly coincides with the maximum of the Mn L_3 absorption edge, which corresponds to the maximum in the empty Mn $3d$ DOS. The origin of such a large effect of reemission is closely connected to peculiarities of the electronic structure in half-metallic ferromagnets. The long lifetime of the excited states (which is necessary for intense reemission) is provided by the suppression of nonradiative relaxation of excited electrons near the Fermi level and by their prolonged stay on an excited atom due to the field of the core hole. In Heusler alloys having large local magnetic moments, there is a possibility of revealling such a mechanism of the relaxation suppression. This possibility is based on strong exchange splitting, which is typical for systems with the half-metallic ferromagnet DOS structure. Both the existence of the energy gap for the spin-down projection of Mn $3d$ states and the weak hybridization of Mn $3d$ electrons with nearest neighbors lead to the suppression of the excited electron relaxation. Therefore our findings can be fully interpreted in terms of the half-metallic character of the electronic structure of Heusler alloys.

A theoretical model for the description of resonance scattering of polarized x rays is proposed and a simple quantitative theory of magnetic circular dichroism in x-ray emission in terms of the spin-polarized electron density of states is developed.

Note that further investigations on this subject would be very useful, e.g., for studying magnetic dichroism in materials having a large local magnetic moment at an atomic site.

ACKNOWLEDGMENTS

This work was supported by the Russian Science Foundation for Fundamental Research (Projects No. 00-1596575 and No. 99-02-16268), a NATO Collaborative Linkage Grant the Swedish Natural Science Research Council (NFR), the Goran Gustavsson Foundation in Natural Sciences and Medicine, Deutsche Forschungsgemeinschaft DFG Project No. Br 1184/4, and Bundesministerium fur Bildung und Forshung (Grant No. BMFB 05SB8MPB8). We thank C. F. Hague for lending equipment. The Technical assistance of the ESRF staff is gratefully acknowledged. The single crystal of NiMnSb was supplied by Ch. Hordequien (CNRS) and polycrystalline Co_2MnSb was supplied by Elena I. Shreder (Institute of Metal Physics, Russian Academy of Sciences, Ural Division) The authors are grateful to A. Postnikov and M. Magnuson for carefully reading the manuscript.

APPENDIX: MATHEMATICAL MODEL

The intensity of resonant x-ray emission induced by photons of energy $\hbar\omega$ and polarization q is given by

$$I_q^e(\omega',\omega) \propto \sum_{q'} F_{q'q}, \tag{A1}$$

where the summation is over the polarization directions q' of emitted photons with energy $\hbar\omega'$. The intensity of photons with the polarization $q=(+1,0,-1)$ scattered into a state with polarization q' is given by the Kramers-Heisenberg formula

$$F_{q'q} = \sum_f \left| \sum_x \frac{\langle \Phi_f | C_{q'} | \Phi_x \rangle \langle \Phi_x | C_q | \Phi_0 \rangle}{E_0 + \hbar\omega - E_x - i\Gamma_x} \right|^2 \times \delta(E_f + \hbar\omega' - E_0 - \hbar\omega). \tag{A2}$$

Here, Φ_0 is the ground state of an electron system with energy E_0. Φ_x is an excited (by absorption of a photon) state with energy E_x and damping Γ_x. The outer summation over the final states Φ_f is constrained by the δ function representing the energy conservation law. For damped final states the δ function should be substituted by a Lorentz function with FWHM Γ_f.

The dipole transition operator C_q is expressed via spherical harmonics with the orbital moment $l=1$ and projections $m=0,\pm 1$,

$$C_{\pm 1} = (x \pm iy)/\sqrt{2} = \mp \sqrt{4\pi/3} r Y_{1,\pm 1},$$

$$C_0 = z = \sqrt{4\pi/3} r Y_{1,0}, \tag{A3}$$

where the z direction is along the spin axis of the solid.

In the Mn atom, the $2p$ inner states are split by the spin-orbit interaction (12 eV) into two groups with total moments $j=l+s$ equal to 1/2 and 3/2. Their angular and spin parts are

TABLE II. Squared angular parts of the dipole matrix elements between inner Φ_c and valence $\Phi^{\downarrow}_{i\mathbf{k}}$ states (in units of $R^2/15$).

Φ_c	m_j	$\lvert\langle\Phi^{\downarrow}_{i\mathbf{k}}\rvert C_{+1}\rvert\Phi_c\rangle\rvert^2$	$\lvert\langle\Phi^{\downarrow}_{i\mathbf{k}}\rvert C_{-1}\rvert\Phi_c\rangle\rvert^2$	$\lvert\langle\Phi^{\downarrow}_{i\mathbf{k}}\rvert C_{0}\rvert\Phi_c\rangle\rvert^2$
$2p_{1/2}$	$-1/2$	$\lvert a_1\rvert^2$	$\lvert a_{-1}\rvert^2$	$(4/3)\lvert a_0\rvert^2$
	$1/2$	$4\lvert a_2\rvert^2$	$(2/3)\lvert a_0\rvert^2$	$2\lvert a_1\rvert^2$
$2p_{3/2}$	$-3/2$	$\lvert a_0\rvert^2$	$6\lvert a_{-2}\rvert^2$	$3\lvert a_{-1}\rvert^2$
	$-1/2$	$2\lvert a_1\rvert^2$	$2\lvert a_{-1}\rvert^2$	$(8/3)\lvert a_0\rvert^2$
	$1/2$	$2\lvert a_2\rvert^2$	$(1/3)\lvert a_0\rvert^2$	$\lvert a_1\rvert^2$
	$3/2$	0	0	0

$$\Phi_{1/2,1/2}=\frac{1}{\sqrt{3}}(Y^{\uparrow}_{10}-\sqrt{2}Y^{\downarrow}_{11}),$$

$$\Phi_{1/2,-1/2}=\frac{1}{\sqrt{3}}(\sqrt{2}Y^{\uparrow}_{1-1}-Y^{\downarrow}_{10}), \tag{A4}$$

$$\Phi_{3/2,1/2}=\frac{1}{\sqrt{3}}(\sqrt{2}Y^{\uparrow}_{10}+Y^{\downarrow}_{11}),$$

$$\Phi_{3/2,-1/2}=\frac{1}{\sqrt{3}}(Y^{\uparrow}_{1-1}+\sqrt{2}Y^{\downarrow}_{10}),$$

$$\Phi_{3/2,3/2}=Y^{\uparrow}_{11},\quad \Phi_{3/2,-3/2}=Y^{\downarrow}_{1-1}, \tag{A5}$$

where the arrows stand for spin functions.

One can expand the valence states $\Phi^{s}_{i\mathbf{k}}$ (i numbers the bands, $\mathbf{k}$ is the wave vector, $s=\uparrow,\downarrow$) over spherical harmonics Y^{s}_{lm} centered at the excited atom,

$$\Phi^{\downarrow}_{i\mathbf{k}}(\mathbf{r})=\sum_{lm} a^{\downarrow}_{lm,ik}R_{\epsilon l,i\mathbf{k}}Y^{\downarrow}_{lm} \tag{A6}$$

(and correspondingly for the spin-up states). Here, $R_{\epsilon l,i\mathbf{k}}$ is a (possibly spin-dependent) radial part of the solution of the Schrödinger equation inside the muffin-tin sphere with orbital moment l and energy $\epsilon=\epsilon_{i\mathbf{k}s}$. The expansion coefficients $a^{s}_{lm,i\mathbf{k}}$ are determined from corresponding band structure calculations.

In Table II, the squared angular parts of the transition matrix elements $\lvert\langle\Phi^{\downarrow}_{i\mathbf{k}}\rvert C_q\rvert\Phi_c\rangle\rvert^2$ from inner states Φ_c into valence ones $\Phi^{\downarrow}_{i\mathbf{k}}$ are shown for $l=2$. For brevity, band indices $i\mathbf{k}$ and the index $l=2$ are dropped. Let us restrict ourselves to discussion of the p-d transitions only. The full matrix elements are in this case obtained by multiplication by the squared absolute value of the radial matrix element

$$R=\int R_{\epsilon l,i\mathbf{k}}(r)R_{21}(r)r^3dr \tag{A7}$$

between a core-level state R_{nl} ($n=2,l=1$) and a valence state [Eq. (A6)]. The corresponding matrix elements of the transitions in the spin-up states can be found from Table II by making use of the relations

$$\lvert\langle\Phi^{\uparrow}_{i\mathbf{k}}\rvert C_q\rvert\Phi_{jm_j}\rangle\rvert^2=\lvert\langle\Phi^{\downarrow}_{i\mathbf{k}}\rvert C_{-q}\rvert\Phi_{j-m_j}\rangle\rvert^2. \tag{A8}$$

Simultaneous inversion of all directions does not affect the transfer probabilities.

$$g^{\downarrow}_l(\epsilon)=\frac{1}{(2l+1)N}\sum_{i\mathbf{k},m}\lvert a^{\downarrow}_{lm,i\mathbf{k}}\rvert^2\delta(\epsilon-\epsilon^{\downarrow}_{i\mathbf{k}}) \tag{A9}$$

is the partial density of states of symmetry l, calculated per l state per atom. The calculated partial densities of d states per Mn atom in NiMnSb are shown in Fig. 5.

1. Emission

Let us separate the emission process into two parts: (i) the emission as such, understood as the radiation due to the transition from electron states below the Fermi energy ϵ_{F}, and (ii) resonant elastic scattering of photons, known as reemission.

In the first of these processes, an electron from an inner state Φ_c due to an absorption of an incident photon with polarization q and energy $\hbar\omega$ is transferred into an empty band state $\Phi^{s}_{i\mathbf{k}}$. Then, another electron from a state $\Phi^{s'}_{i'\mathbf{k}'}$ with energy $\epsilon<\epsilon_{\mathrm{F}}$ fills the created hole, emitting another photon with polarization q' and energy $\hbar\omega'$. The electron-hole pair $(i'\mathbf{k}'s',i\mathbf{k}s)$ emerging in the final state determines the photon energy loss after being scattered.

Using the data listed in Table II one can find, for example, the intensity of emission with linear polarization $q'=0$ due to the excitation of an electron from the $2p_{1/2}$ shell by a right-hand polarized photon $q=1$ with the creation of an electron-hole pair with spins $\uparrow\downarrow$:

$$F^{\uparrow\downarrow}_{01}=\frac{R^4}{15^2}\sum_{i\mathbf{k}i'\mathbf{k}'}\left|\frac{\sqrt{2}a^{\uparrow}_{-1}a^{\downarrow *}_{1}+\sqrt{\frac{4}{3}}a^{\uparrow}_{0}2a^{\downarrow *}_{2}}{\epsilon-\epsilon^{\downarrow}_{i\mathbf{k}}-i\Gamma_x}\right|^2\delta(\epsilon'-\epsilon^{\uparrow}_{i'\mathbf{k}'}) \tag{A10}$$

$$=R^4\frac{\pi}{15^2\Gamma_x}7\frac{1}{3}g^{\uparrow}(\epsilon'-i\Gamma_f)g^{\downarrow}(\epsilon-i\Gamma_x). \tag{A11}$$

Here $\epsilon=\hbar\omega-\lvert E_{2p_{1/2}}\rvert,\epsilon'=\hbar\omega'-\lvert E_{2p_{1/2}}\rvert$. The first term in the numerator describes the excitation amplitude into a state with total moment projection $m_j=\frac{1}{2}$ and the second one into a state with $m_j=-\frac{1}{2}$.

Assuming approximate diagonality of the sum

$$\sum_{i\mathbf{k}} a^{\downarrow}_{m,ik}a^{\downarrow *}_{m',ik}\delta(\epsilon-\epsilon_{ik})\propto\delta_{mm'}, \tag{A12}$$

one notices that in the calculation of the squared amplitudes in Eq. (A10) the cross terms disappear. Equation (A10) was obtained assuming that there is no dependence of the radial matrix elements on energy, band number, and spin index. The densities of states $g(\epsilon-i\Gamma)$ take into account the damping of the intermediate Γ_x states (those with the hole in the inner shell) and of the final Γ_f states. In the following, we drop the imaginary parts of the energies ϵ and ϵ'.

TABLE III. Transition probability between inner states Φ_c and valence states of energy ϵ (in units of $R^2/15$).

Φ_c	m_j	$f_{+1}^{m_j}$	$f_{-1}^{m_j}$	$f_0^{m_j}$
$2p_{1/2}$	$-1/2$	$g_1^{\downarrow}+(2/3)g_0^{\uparrow}$	$g_{-1}^{\downarrow}+4g_{-2}^{\uparrow}$	$(4/3)g_0^{\downarrow}+2g_{-1}^{\uparrow}$
	$1/2$	$4g_2^{\downarrow}+g_1^{\uparrow}$	$(2/3)g_0^{\downarrow}+g_{-1}^{\uparrow}$	$2g_1^{\downarrow}+(4/3)g_0^{\uparrow}$
$2p_{/32}$	$-3/2$	$g_0^{\downarrow}$	$6g_{-2}^{\downarrow}$	$3g_{-1}^{\downarrow}$
	$-1/2$	$2g_1^{\downarrow}+(1/3)g_0^{\uparrow}$	$2g_{-1}^{\downarrow}+2g_{-2}^{\uparrow}$	$(8/3)g_0^{\downarrow}+g_{-1}^{\uparrow}$
	$1/2$	$2g_2^{\downarrow}+2g_1^{\uparrow}$	$(1/3)g_0^{\downarrow}+2g_{-1}^{\uparrow}$	$g_1^{\downarrow}+(8/3)g_0^{\uparrow}$
	$3/2$	$6g_2^{\uparrow}$	$g_0^{\uparrow}$	$3g_1^{\uparrow}$

The total intensity of the emission process is obtained by summation over final states with all possible spin projections. In order to simplify this procedure, we introduce the quantity

$$f_q^c(\epsilon)=\frac{1}{N}\sum_{i\mathbf{k}s}|\langle\Phi_{i\mathbf{k}}^s|C_q|\Phi_c\rangle|^2\delta(\epsilon-\epsilon_{i\mathbf{k}}^s), \qquad \text{(A13)}$$

where $c=j,m_j$, which is essentially the probability of absorbing a photon with polarization q in the course of excitation from a particular inner state Φ_c.

In Table III, all values of this quantity are expressed via the special densities of states

$$g_m^s(\epsilon)=\frac{1}{N}\sum_{i\mathbf{k}}|a_{m,i\mathbf{k}}^s|^2\delta(\epsilon-\epsilon_{i\mathbf{k}}^s), \quad s=\uparrow,\downarrow. \qquad \text{(A14)}$$

In the following we substitute their mean values (A9), i.e., the spin-resolved partial densities of states. In other words, we neglect the $3d$ spin-orbit interaction compared with exchange interaction. This approximation is reasonable in our case. It allows us to obtain simple equations for resonant x-ray scattering.

In the notation (A13), the intensity of photon scattering $q,\epsilon\rightarrow q',\epsilon'$ assumes the form

$$F_{q'q}^e(\epsilon',\epsilon)=\frac{R^4}{15^2}\frac{\pi}{\Gamma_x}\sum_{m_j}f_{-q'}^{m_j}(\epsilon')f_q^{m_j}(\epsilon), \qquad \text{(A15)}$$

and the absorption spectrum is given by

$$F_q^a(\epsilon)=\frac{R^2}{15}\sum_{m_j}f_q^{m_j}(\epsilon). \qquad \text{(A16)}$$

The intensities of inelastic photon scattering with different polarizations $F_{qq'}^e$ [Eq. (A15)] make it possible to find the angular dependence of emission. In order to keep the mathematics simple, let us assume that all directions of polarization of the emitted photons enter with equal weights, i.e., we consider the emission

$$I_+^e=\frac{2}{3}(F_{-11}^e+F_{01}^e+F_{11}^e). \qquad \text{(A17)}$$

Equation (A17) is exact for the ''magic'' angle 55° between photon direction and magnetization axis, or for angle integrated emission. The main results obtained for the case (A17) remain valid for the general case as well.

In order to study the effect of spin polarization, it is convenient to introduce symmetric and antisymmetric components of the partial density of states, $g_{s,a}(\epsilon)=[g^{\uparrow}(\epsilon)\pm g^{\downarrow}(\epsilon)]/2$. With the help of Eqs. (A15) and (A17) and Table I we arrive at the emission intensities in the course of resonant excitation by right-hand polarization, in the case when the photon helicity is parallel to the spin of the excited atom:

$$^{1/2}I_+^e(\epsilon')=\left(\frac{2R^2}{9}\right)^2\frac{2}{3}\frac{\pi}{\Gamma_x}[6g_s(\epsilon')g_s(\epsilon)+0.8g_a(\epsilon')g_a(\epsilon) -g_a(\epsilon')g_s(\epsilon)-3g_s(\epsilon')g_a(\epsilon)], \qquad \text{(A18)}$$

$$^{3/2}I_+^e(\epsilon')=\left(\frac{2R^2}{9}\right)^2\frac{2}{3}\frac{\pi}{\Gamma_x}[12g_s(\epsilon')g_s(\epsilon)+6.8g_a(\epsilon')g_a(\epsilon) +5g_a(\epsilon')g_s(\epsilon)+3g_s(\epsilon')g_a(\epsilon)]. \qquad \text{(A19)}$$

The damping of the excited states Γ_x is determined primarily by the inverse lifetime of the core hole Γ_c.

The absorption spectra are given by

$$^{1/2}I_+^a(\epsilon)=\frac{2R^2}{9}[2g_s(\epsilon)-g_a(\epsilon)], \qquad \text{(A20)}$$

$$^{3/2}I_+^a(\epsilon)=\frac{2R^2}{9}[4g_s(\epsilon)+g_a(\epsilon)]. \qquad \text{(A21)}$$

The emission and absorption spectra in the case of excitation by left-hand polarized radiation ($q=-1$) follow from Eqs. (A18)–(A21) when g_a is substituted by $-g_a$. In the case of nonpolarized incident radiation, the third and fourth terms in Eqs. (A18) and (A19) disappear as they are odd in g_a. However, the effect of spin polarization on the emission, i.e., the second term, remains substantial. In the case of opposite spin polarizations of occupied and vacant states the emission is weakened; for parallel spin polarizations the emission is enhanced.

2. Reemission

In resonant elastic scattering, the initial and final states of the electron system are identical. The energies of incident and emitted photons are equal, but their polarizations may differ. A given final state may be achieved via different paths, for example, through excitation from one of two or one of four inner states for $2p_{1/2}$ and $2p_{3/2}$ shells, respectively. Consequently, one must add the amplitudes of possible transitions rather than their probabilities.

In the approximations adopted above, the main formula for the intensity of reemission affected by diagonal components only reads

$$F_{qq}^r(\epsilon)=\frac{R^4}{15^2}\frac{\pi}{\Gamma^*}\left(\sum_{m_j}f_q^{m_j}(\epsilon)\right)^2. \qquad \text{(A22)}$$

Hence the reemission is proportional to the square of the absorption intensity for a given energy. Making use of Table III we obtain

$$^{1/2}I_{+}^{r}(\epsilon)=\left(\frac{2R^2}{9}\right)^2\frac{2}{3}\frac{\pi}{\Gamma^*}[4g_s^2(\epsilon)+g_a^2(\epsilon)-4g_s(\epsilon)g_a(\epsilon)], \tag{A23}$$

$$^{3/2}I_{+}^{r}(\epsilon)=\left(\frac{2R^2}{9}\right)^2\frac{2}{3}\frac{\pi}{\Gamma^*}[16g_s^2(\epsilon)+g_a^2(\epsilon)+8g_s(\epsilon)g_a(\epsilon)]. \tag{A24}$$

The intensity of reemission for excitation by left-hand polarized radiation ($q=-1$) is again obtained by substituting g_a by $-g_a$.

The formulas (A22)–(A24) for reemission resemble those for conventional emission and absorption. One should remember, however, that the reemission occurs from an excited free state with damping Γ_r whereas in conventional emission, i.e., from the states below the Fermi level, the damping of the latter is negligible. The damping in absorption and emission spectra is determined by a core hole, $\Gamma_x=\Gamma_c$, while in case of reemission $\Gamma_x=\Gamma_r+\Gamma_c$, where Γ_r accounts for inelastic processes and moreover for the probability for an excited electron to leave the atom completely.

For peak-shaped functions the following relation approximately holds:

$$g(\epsilon-i\Gamma_x)\simeq\frac{\Gamma_c}{\Gamma_x}g(\epsilon-i\Gamma_c).$$

This was used to introduce the quantity $1/\Gamma^*=(1/\Gamma_f)[\Gamma_c/(\Gamma_c+\Gamma_r)]^2$ in Eq. (A22).

*On leave from the X-ray Spectroscopy Laboratory, Institute of Metal Physics, Russian Academy of Sciences–Ural Division, Ekaterinburg, Russia.

[1] J. Erskine and E. Stern, Phys. Rev. B **12**, 5016 (1975).

[2] G. van der Laan, B.T. Thole, G.A. Sawatzky, J.B. Goedkoop, J.C. Fuggle, J.-M. Esteva, R. Karnatak, J.P. Remaika, and H. Dabkowska, Phys. Rev. B **34**, 6529 (1986).

[3] G. Schnütz, W. Wagner, W. Wilhelm, P. Kienle, R. Zeller, R. Frahm, and G. Materlik, Phys. Rev. Lett. **58**, 737 (1987).

[4] G. Schnütz, M. Knulle, R. Wienke, W. Wilhelm, W. Wagner, P. Kienle, and R. Frahm, Z. Phys. B: Condens. Matter **73**, 67 (1988).

[5] B.T. Thole, P. Carra, F. Sette, and G. van der Laan, Phys. Rev. Lett. **68**, 1943 (1992).

[6] P. Carra, B.T. Thole, M. Altarelli, and X. Wang, Phys. Rev. Lett. **70**, 694 (1993).

[7] J. Stöhr and Y. Wu, in *New Directions in Research with 3rd Generation Soft X-Ray Syncrotron Radiation Sources*, Vol. 254 of *NATO Advanced Study Institute, Series E: Applied Sciences*, edited by A.S. Schlachter and F.J. Wuilleumier (Kluwer Academic, Dordrecht, Netherlands, 1994), p. 221.

[8] L.-C. Duda, J. Electron Spectrosc. Relat. Phenom. **110-111**, 287 (2000).

[9] P. Strange, P.J. Durham, and B.L. Gyorffy, Phys. Rev. Lett. **67**, 3590 (1991).

[10] C.F. Hague, J.-M. Mariot, P. Strange, P.J. Durham, and B.L. Gyorffly, Phys. Rev. B **48**, 3560 (1993).

[11] C.F. Hague, J.M. Mariot, G.Y. Guo, K. Hricovini, and G. Krill, Phys. Rev. B **51**, 1370 (1995).

[12] L.-C. Duda, J. Stöhr, D.C. Manchini, A. Nilsson, N. Wassdahl, J. Nordgren, and M.G. Samant, Phys. Rev. B **50**, 16 758 (1994).

[13] C.F. Hague, J.-M. Mariot, and J.-J. Gallet, Appl. Phys. A: Mater. Sci. Process. **65**, 141 (1997).

[14] L. Braicovich, C. Dallera, G. Ghiringhelli, N.B. Brookes, and J.B. Goedkoop, Phys. Rev. B **55**, R14 729 (1997).

[15] U. Pustogowa, L. Szunyogh, H. Ebert, and P. Weinberger, Solid State Commun. **108**, 343 (1997).

[16] J.-J. Gallet, J.-M. Mariot, L. Journel, C.F. Hague, J.P. Kappler, G. Schmerber, D.J. Singh, D. Krill, J. Goulon, and A. Rogalev, Phys. Rev. B **57**, 7835 (1998).

[17] T. Jo and J.-C. Parlebus, J. Phys. Soc. Jpn. **68**, 1392 (1999).

[18] P. Kuiper, J. Phys. Soc. Jpn. **69**, 874 (2000).

[19] R.A. de Groot, F.M. Mueller, P.G. van Engen, and K.H.J. Buschow, Phys. Rev. Lett. **50**, 2024 (1983).

[20] L. Braicovich and G. Ghiringhelli, Phys. Rev. B **58**, 6688 (1998).

[21] F. Heusler, Verh. Dtsch. Phys. Ges. **5**, 219 (1903).

[22] P. J. Webster, J. Phys. Chem. Solids **32**, 1221 (1971).

[23] J. Kübler, A. Williams, and C. Sommers, Phys. Rev. B **28**, 1745 (1983).

[24] S. Ishida, S. Fujii, S. Kawhiwagi, and S. Asano, J. Phys. Soc. Jpn. **64**, 2152 (1995).

[25] Yu.M. Yarmoshenko, M.I. Katsnelson, E.I. Shreder, E.Z. Kurmaev, A. Slebarski, S. Plogmann, T. Schlathölter, J. Braun, and M. Neumann, Eur. Phys. J. B **2**, 1 (1998).

[26] S. Plogmann, T. Schlathölter, J. Braun, M. Neumann, Y.M. Yarmoshenko, M.V. Yablonskikh, E.I. Shreder, E.Z. Kurmaev, A. Wrona, and A. Ślebarski, Phys. Rev. B **60**, 6428 (1999).

[27] J. Goulon, N.B. Brookes, C. Gauthier, J.B. Goedkoop, C. Goulon-Ginet, M. Hagelstein, and A. Rogalev, Physica B **199**, 199 (1995).

[28] P. Elleaume, J. Synchrotron Radiat. **1**, 19 (1994).

[29] J. Nordgren, B. Gray, S. Cramm, R. Nyholm, J.-E. Rubenson, and N. Wassdahl Rev. Sci. Instrum. **60**, 1690 (1989).

[30] A. Kimura, S. Suga, T. Shishidou, S. Imada, T. Muro, S.Y. Park, T. Miyahara, T. Kaneko, and T. Kanomata, Phys. Rev. B **56**, 6021 (1997).

[31] A.N. Titov, A.V. Kuranov, V.G. Pleschev, Yu.M. Yarmoshenko, M.V. Yablonskikh, A.V. Postnikov, S. Plogmann, M. Neumann, A.V. Ezhov, and E.Z. Kurmaev, Phys. Rev. B **63**, 035106 (2001).

[32] S. Plogmann, Ph.D. thesis, University of Osnabrück, 1999.

[33] C.-O. Almbladh and L. Hedin, *Handbook on Synchrotron Radiation* (North-Holland, Amsterdam, 1983), Vol. 1, p. 607.

[34] V. Grebennikov, Y. Babanov, and O. Sokolov, Phys. Status Solidi B **80**, 73 (1977).

[35] O. Sokolov, V. Grebennikov, and E. Turov, Phys. Status Solidi B **83**, 383 (1977).